Reconstructing magnetic fields of spiral galaxies from radiopolarimetric observations

Shneider, C.

1

Introduction

> "The argument in the past has frequently been a process of elimination: one observed certain phenomena, and one investigated what part of the phenomena could be explained; then the unexplained part was taken to show the effects of the magnetic field. It is clear in this case that, the larger one's ignorance, the stronger the magnetic field."
>
> — Lodewijk Woltjer, Remarks[1] on the Galactic Magnetic Field, 1967.

1.1 Prelude

Galactic magnetic fields have come a long way; from being avoided for their complexity or naively invoked to explain cosmic phenomena, they are now established as a major and ubiquitous constituent of galaxies and form part of the broader, rapidly expanding field of Cosmic Magnetism. In fact, in the fast approaching era of 'mega-telescopes', ***magnetism*** is explicitly named as key science for the current LOw Frequency ARray (LOFAR) and future Square Kilometre Array (SKA) radio telescopes. It is Radio Astronomy that reveals the nature of magnetic fields in the cosmos as most of the tracers of cosmic magnetism lie in the radio domain. For example, the already operational Karl G. Jansky Very Large Array (VLA), LOFAR, and Atacama Large Millimeter/submillimeter Array (ALMA) are all able to provide detailed characterization of magnetic fields. The SKA with its two precursors, the Australian Square Kilometre Array Pathfinder (ASKAP) and the Meer ('more of') Karoo Array Telescope (MeerKAT), will provide unprecedented sensitivity and resolution, thereby revolutionizing the study of magnetic fields not only in our own

[1] Proceedings from IAU Symposium no. 31 held in Noordwijk, Netherlands.

Galaxy but also in external galaxies, the intracluster medium (ICM), and the intergalactic medium (IGM).

Although magnetic fields do not sculpt the dynamics of galaxies on the whole, they carry significant energy, not only in galaxy disks but also in galaxy halos (Haverkorn & Heesen 2012), and exert influence on virtually all astrophysical processes in the interstellar medium (ISM) (Ferrière 2001; Landecker 2012; Haverkorn 2014) and, consequently, influence galactic evolution.

Detailed knowledge of galactic magnetic fields is beneficial for ISM and star formation studies, as a significant foreground for studies of the Cosmic Microwave Background (CMB) B-mode polarization, the Epoch of Reionization (EoR), and magnetization of the cosmic web, and for tracing the arrival directions of Ultra high energy Cosmic Rays (UHECRs).

In the next section, the key constituent interactions in the ISM are presented and discussed. This is followed by a discussion of the energy spectrum of turbulence and the classification of magnetic fields according to field types. The synchrotron radiation mechanism is subsequently discussed followed by radio observables and polarization. Finally the current status of magnetic field knowledge is addressed, including the inferred dominant magnetic field modes in galaxy disks and halos, and the contribution of this thesis to galactic magnetism is summarized.

1.2 The interactive ISM

The ISM is broadly composed of gas, magnetic fields, cosmic rays (CRs), and dust. The gaseous phase of the ISM is classically composed of four phases, either ionized or neutral (for a review see Ferrière (2001)). The neutral phases are the Cold and Warm Neutral Media (CNM and WNM) and consist of atoms (predominantly hydrogen and helium with traces of metals) and molecules. The ionized phases are the Warm and Hot Ionized Media (WIM and HIM). In this thesis, the WIM is the relevant gas phase; ionized gas at a temperature of $\sim$ 8000 K and density 0.1 cm^{-3} (Tielens 2005), volume filling factor of $f_{\rm V}$ $\sim$ 20% and mass filling factor of $f_{\rm m} \sim$ 10%. The WIM is very inhomogeneous and almost fully ionized ($\sim$ 0.9). Ionizing photons from O stars are the main source of ionization of the WIM. There are low-density channels that enable these ionizing photons from the O stars in the stellar disk to travel from the disk to far above the galactic mid-plane. This results in a large scale height of the WIM of about 1 kpc. The ionized gas is tightly coupled to the magnetic field and motions of the plasma can function to regenerate the large-scale magnetic field, converting kinetic energy into magnetic energy. Such a mechanism is known as a dynamo.

CRs are comprised of relativistic electrons (CREs), protons, and atomic nuclei, which have a power-law energy spectrum ranging from (at least) 10^{10} eV to $\sim 10^{20}$ eV. A slight break in the spectral slope occurs at about $10^{17.5}$ eV, thought to coincide with a transition from lower-energy Galactic CRs to higher-energy extragalactic CRs. These high-energy CRs can not be of Galactic origin since their Larmor radius exceeds the thickness of the Galaxy disk which allows them to immediately escape from the Milky Way. CREs

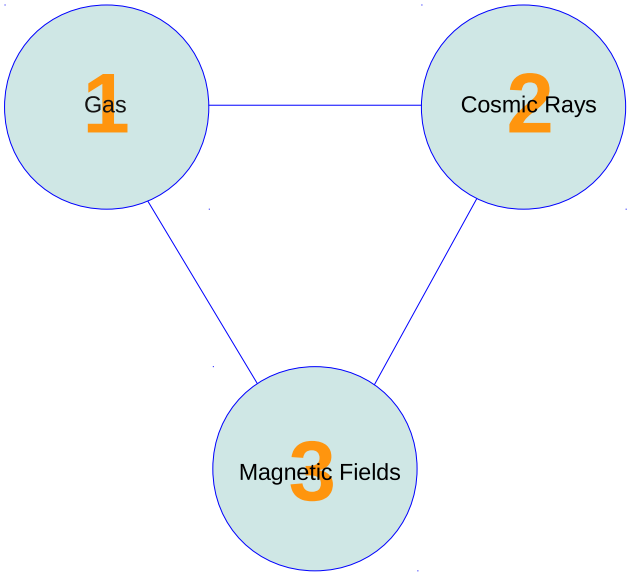

Figure 1.1: The ISM network described by gas, cosmic rays, and magnetic fields. The connecting edges denote bidirectional interaction.

spiraling around Galactic magnetic field lines emit synchrotron radiation detectable in the radio regime. In this way, CRs diffuse through the ISM with a diffusion coefficient given as the ratio of the mean-free path traveled by a CRE from its origin in the plasma to its synchrotron lifetime.

In the ISM, the energy densities of the turbulent gas, thermal gas, magnetic field and cosmic ray electrons are all on the order of ≈ 1 eV cm^{-3} (Hennebelle & Falgarone 2012), implying that all these processes are dynamically important and provide significant feedback on each other. We now provide examples of the feedback functionality of these three components as it operates in the ISM, shown schematically in Fig. 1.1.

1 → 2:
CRs are accelerated in astrophysical shocks found in objects such as supernova remnants (SNRs) through Fermi acceleration as proposed by E. Fermi in 1949. Acceleration continues as long the magnetic field is able to contain the CRs within the shocked region.

1 → 3:
At the same time, turbulent motions also amplify and distort magnetic fields and enhance magnetic diffusion. Plasma motions on a sufficiently large scale actuate the $\alpha - \omega$ (alpha-omega) dynamo (Parker 1955). The weight of the ordinary matter serves to confine the magnetic fields.

2 → 1:
CRs heat dense interstellar clouds that are too dense for photons to penetrate. They also drive galactic winds (Breitschwerdt et al. 1991, 1993). Also, the interaction of CRs with interstellar gas and dust produces gamma rays.

2 → 3:
CR driven dynamo (Parker 1992; Hanasz et al. 2004; Kulpa-Dybeł et al. 2015) and CR pressure inflates buoyant loops of magnetic fields via the Parker instability (magnetic buoyancy instability) (Parker 1966).

3 → 1:
Magnetic fields affect charged particles via the Lorentz force and can accelerate charged particles to high energies. They couple with both charged and neutral particles, via ion-neutral collisions, except for the densest parts of molecular clouds (Ferrière 2001), participate in gas dynamics, regulate cloud collapse and the subsequent onset of star formation, and affect motions of supernova remnants and bubbles (e.g., see Wolleben et al. (2010); Iacobelli et al. (2013)).

3 → 2:
Magnetic fields regulate the energy and distribution of CR; they affect CR diffusion length and diffusion time scales (Beck 2004). The diffusion coefficient varies with magnetic field strength and the field's degree of ordering. For example, Mulcahy et al. (2014) suggest that the CRE diffusion coefficient in M51 could be lower than in the Milky as a result of M51 having a stronger and possibly more turbulent magnetic field. Moreover, magnetic fields both decelerate CR, causing energy loss through emission of synchrotron radiation and accelerate CR via the mechanism of Fermi acceleration.

1.2.1 Turbulent energy spectrum

Turbulence is a property of a random, (fluid) flow characterized by spectral energy transfer that proceeds through non-linear, multi-scale interactions. In fact, from the electron density power spectrum of the WIM, turbulence in the WIM spans at least 10 decades of scale from 10^{-3} AU $\lesssim l \lesssim$ 100 pc (Armstrong et al. 1995).

The magnetized, multi-phase ISM is randomly stirred on the largest scales, most vigorously by old SNRs in the disk and by superbubbles and Parker instability in the halo, as shown by Mao et al. (2015) for M51. SNe input 10^{51} ergs (10^{44} J) per event resulting in an expanding SNR. After $\approx$ 1 Myr, the SNR's expansion speed has reduced to the ISM sound speed of $c_s \approx 10$ km s^{-1}, the size of the SNR has reached 50 – 100 pc at pressure balance, and SN shell merger with the ISM has commenced.

Although a gross simplification of the actual turbulence in the ISM, which requires a detailed description of the astrophysical plasma, magnetohydrodynamics (MHD) can be used as a clean dynamical theory to treat non-relativistic and slowly varying motions

(on time scales much longer than the inverse of the plasma frequency) of the highly-conducting plasma. This plasma is assumed to be subject only to the action of mechanical and magnetic forces. As magnetic fields are stretched and bent by the turbulent motions in the ISM, they resist deformation via magnetic tension. Thus, from the combined action of the turbulent advection of the magnetic field and the field's back reaction, a statistically steady state of (incompressible) MHD turbulence can be assumed to arise which is then characterized by a power-law energy spectrum (Schekochihin & Cowley 2007).

Three main regimes for this energy-spectrum hold:

1. Integral scale: The driving force of turbulence injects energy and momentum into the largest eddies (cells) comparable to the object size. Turbulent motions decay at the turnover time of the largest eddy.

2. Inertial range: An energy cascade ensues, subject to inertial forces, with energy progressively removed from larger eddies (small k) and deposited at small eddies (large k) where k is the wavenumber ($2\pi/l$). Kinetic energy is conserved (does not dissipate). The energy transfer rate proceeds independently of k, with the eddies unaware of either the driving force or of dissipation. There is thus a power law dependence of $E(k)$ on k which translates to a linear relationship in $\log E(k)$ vs $\log k$.

3. Dissipation scale: Energy is transferred to heat by viscous forces, marking the end of the inertial range.

As proof of the necessity for dynamo action in the ISM, we briefly consider the fundamental MHD equation which describes the time evolution of the magnetic field as

$$\frac{\partial \mathbf{B}}{\partial t} = \nabla \times (\mathbf{v} \times \mathbf{B}) + \eta \nabla^2 \mathbf{B}, \tag{1.1}$$

where $\mathbf{B} = \overline{\mathbf{B}}$ is the total magnetic field set equal to the large-scale field (having assumed the absence of a turbulent magnetic field), $\mathbf{v}$ is the mean velocity, and where η is a constant *Ohmic* magnetic diffusivity depending only on the temperature of the plasma. Moreover, $\eta \propto \sigma^{-1}$, where σ is the electric conductivity. First, consider the idealized case of infinite conductivity, with $\eta = 0$ in the above equation. This yields the so-called ideal MHD equation. The ideal MHD equation describes the 'frozen-in' limit of Eq. (1.1) as a result of magnetic fields moving perfectly with the fluid[2]. As an order of magnitude estimation, the ideal MHD equation can be rewritten as $\tau \approx l/v$ for some characteristic time τ, length l, and velocity v. For $l \sim 100$ pc and velocity equal to c_s, the ideal MHD limit then implies that it would take $\tau \approx 10$ Myr for turbulence to develop in the ISM. Next, without loss of generality, let us assume that the ISM is a static plasma ($\mathbf{v} = 0$) so that only the second term on the right hand side of Eq. (1.1) remains. Thus, we have that $\tau_{\rm diff} \approx l_{\rm diff}^2/\eta$ with a characteristic diffusion time $\tau_{\rm diff}$ and diffusion scale $l_{\rm diff}$. Assuming that charge

[2]Described by Alfvén in 1942 and therefore known as Alfvén's theorem of flux freezing.

Table 1.1: Nomenclature used to describe the three magnetic field types along with a physical basis for these respective fields.

Field type	Regularity	Degree of ordering	Scale	Example causes
Mean, average $\overline{\mathbf{B}}$	regular, uniform	coherent (ordered)	large-scale, global	dynamo action
Anisotropic $\mathbf{b}_{\mathrm{A}}$	random, turbulent, tangled	ordered	small-scale	compression or shear
Isotropic $\mathbf{b}_{\mathrm{I}}$	random, turbulent, tangled	disordered	small-scale	supernovae

separation in the plasma is negligible and that ions and electrons both have a temperature of 10^4 K, yields $\eta \approx 10^7$ cm^2 s^{-1}. Now, with $l_{\mathrm{diff}} \approx 500$ pc for a galactic disk thickness, $\tau_{\mathrm{diff}} \approx 10^{27}$ yr, a time much longer than the age of the universe of 13.7 Gyr. In the real ISM, however, the diffusivity is strongly affected by the turbulent motions of the plasma resulting in the η in Eq. (1.1) being replaced by an isotropic *turbulent* magnetic diffusivity given by $\eta_{\mathrm{turb}} = {}^1\!/_3\, l_{\mathrm{diff}}\, c_s \approx 10^{26}$ cm^2 s^{-1}. This yields a large-scale magnetic field decay time of $\tau_{\mathrm{diff}} \approx 5 \times 10^8$ yr or about ${}^1\!/_{20}$ of the galactic lifetime. Since magnetic fields are indeed observed in galaxies, this, in turn, necessitates dynamo action in the ISM.

1.3 Magnetic field classification

Magnetic fields can be classified according to three distinct field types as described in Table 1.1 and illustrated in Fig. 1.2. Mean or regular fields have sizes of the spiral arms and arise from large-scale motions of the plasma (e.g., differential rotation as part of a dynamo), that drag the essentially 'frozen-in' field lines along. Isotropic turbulent fields, on the other hand, have directions which are completely random. These are fields tangled by supernovae and other outflows such as stellar winds and protostellar outflows. When isotropic turbulent magnetic fields are compressed or sheared by gas flows, they obtain a preferred overall orientation, but with directions remaining frequently reversed on small scales. The circular turbulent cells of the isotropic turbulent field in Fig. 1.2 indicate that the field equally correlates with all spatial directions while the elliptical turbulent cells of the anisotropic turbulent field reflect a stronger spatial correlation along a particular direction.

1.4 Synchrotron radiation

Synchrotron radiation is one of the best tracers of the magnetic field because it is produced throughout the galaxy on account of the Lorentz force. Synchrotron radiation that arises from relativistic cosmic ray electrons is highly linearly polarized, non-thermal continuum emission with flux at cm and m (radio) wavelengths. The ensemble of gyrating cosmic ray electrons in the plasma is assumed to have an isotropic velocity distribution and to

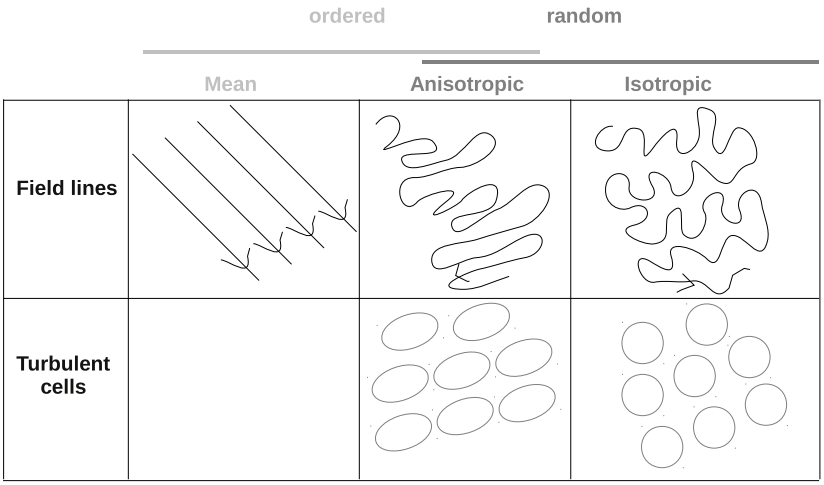

Figure 1.2: Illustrations of field lines and turbulent cells corresponding to the three magnetic field types.

follow a power law energy distribution within a prescribed energy interval. The intensity of synchrotron emission is a measure of the number density of cosmic ray electrons (in the relevant energy range) and of the strength of the total magnetic field in the plane of the sky[3] as illustrated in Fig. 1.3. Furthermore, Fig. 1.3 shows that the signal detected by the radio telescope at a particular wavelength comes from the polarized electric field which serves as a measure of the strength of $B_\perp$. The intrinsic polarization angle is, therefore, perpendicular to the local magnetic field orientation in the sky plane with the electromagnetic wave oscillating along the plane of the E-vector while propagating along $B_\parallel$. Consequently, to indicate the orientation of the headless B-vectors of polarized emission in polarized radio emission maps, the polarization angle of the polarized electric field is rotated by 90°.

1.4.1 Radio observables

Information on magnetic fields, thermal electron density distribution, and cosmic ray electron density distribution is encoded in radio observables. The total synchrotron intensity (Stokes I) is the total synchrotron radiation energy emitted per unit time from the volume enclosed by the telescope beam cylinder. Stokes Q and Stokes U and the polarized intensity (P), with $P = \sqrt{Q^2 + U^2}$, are observables that describe the polarization of the synchrotron radiation. As an example, Fig. 1.4 shows I and P radio synchrotron maps of M51 along with an optical image indicating the B-vectors of polarized emission. To explicitly show how these observables are affected by Faraday rotation it is handy to con-

[3]This is to say that the perpendicular ($B_\perp$) and parallel ($B_\parallel$) to the line-of-sight components of the total magnetic field lie in the sky plane.

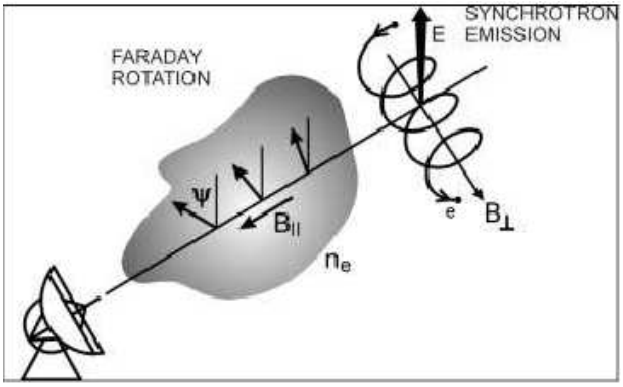

Figure 1.3: Synchrotron emission and Faraday rotation, reproduced from Beck & Wielebinski (2013).

sider the expression for the complex linear polarization of synchrotron emission ($\mathcal{P}$) given by

$$\mathcal{P} = p \exp(2\,\mathrm{i}\,\Psi),$$

where $p = P/I$ is the polarization fraction and Ψ is the observed polarization angle. Faraday rotation causes the intrinsic polarization angle Ψ_0 to rotate along the line of sight as a function of observing wavelength λ as

$$\Psi = \Psi_0 + \mathrm{RM}\,\lambda^2. \tag{1.2}$$

The rotation measure (RM) is given by

$$\left(\frac{RM}{\mathrm{rad\ m^{-2}}}\right) = 0.81 \int_{source}^{\mathrm{telescope}} \left(\frac{n_\mathrm{e}}{\mathrm{cm^{-3}}}\right)\left(\frac{\overline{B}_\parallel + b_\parallel}{\mu\mathrm{G}}\right)\left(\frac{dl}{\mathrm{pc}}\right),$$

where n_e is the thermal electron density, $\overline{B}_\parallel$ is the parallel component of the regular field along the line of sight, $b_\parallel$ is the parallel component of the turbulent field along the line of sight, and dl is an incremental distance along the line of sight from the synchrotron source to the telescope.

With the assumptions pertaining to cosmic ray electrons in Section 1.4, the maximum intrinsic polarization degree p_0 only depends on the spectral index (γ) of the cosmic ray electrons as (Le Roux 1961)

$$p_0 = \frac{\gamma + 1}{\gamma + 7/3}.$$

For typical values of the spectral index γ for spiral galaxies, $p_0 \approx 73\% - 75\%$. However, the actual observed degree of polarization is much lower due to depolarization.

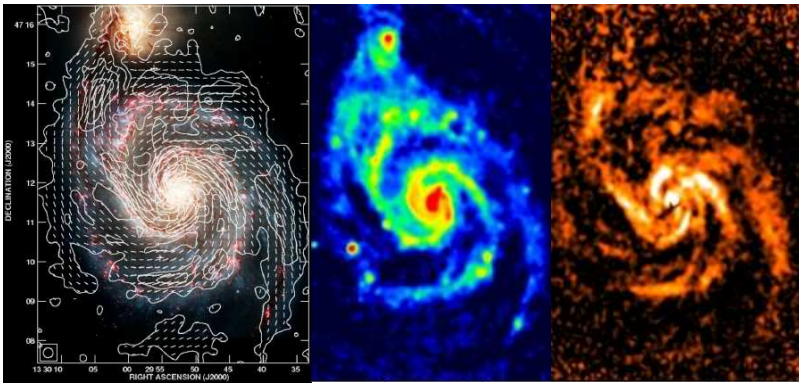

Figure 1.4: All three panels show M51. (Left) Polarized intensity (P) contours are overlaid on a Hubble Space Telescope optical image. Also featured are headless B-vectors of polarized emission with magnitude proportional to the polarized intensity. The polarized radio emission is observed at λ 6.2 cm with 15″ resolution using the VLA and Effelsberg radio telescopes. (Center) Total intensity (I) at λ 6.2 cm at a 8″ resolution. The color scale is in mJy/beam with red indicating higher flux densities per synthesized beam. (Right) Polarized intensity observed at the same wavelength and resolution as the total intensity but now with white indicating higher flux density. All three panels adopted from Fletcher et al. (2011) and the Atlas of Galaxies (MPIfR Bonn) available at http://www.mpifr-bonn.mpg.de.

1.4.2 Polarization

We consider how the distinct magnetic field types, discussed in the preceding section, affect the observed polarization. A starting scenario is to assume a magnetized medium that is devoid of thermal electrons. The variation in intrinsic polarization angle along the line of sight only occurs when a turbulent magnetic field is present as shown by Fig. 1.5. The variation is strongest for a purely isotropic random field and decreases when a regular field is added to this random field as the regular field serves to bring about more order as also shown by Fig. 1.5. As a consequence of the cumulative addition of polarization vectors along the line of sight, a purely mean field preserves the original polarization (no depolarization) while an isotropic random field basically destroys all polarization (complete depolarization). An anisotropic field yields polarization between these two extremes. This is a wavelength-independent depolarization effect as the intrinsic polarization angle is an intrinsic property of the magnetic field configuration.

We now consider thermal electrons in addition to the cosmic ray electrons in the magneto-ionic medium. Now, instead of only having emission along the line of sight, thermal electrons Faraday rotate the E-vector of polarized emission as shown in Fig. 1.3. Consequently, this Faraday rotation gives the strength of $B_{\parallel}$, if the thermal electron density distribution along the line of sight is known, and the direction of $B_{\perp}$. This is a wavelength-dependent effect which increases at longer observing wavelengths.

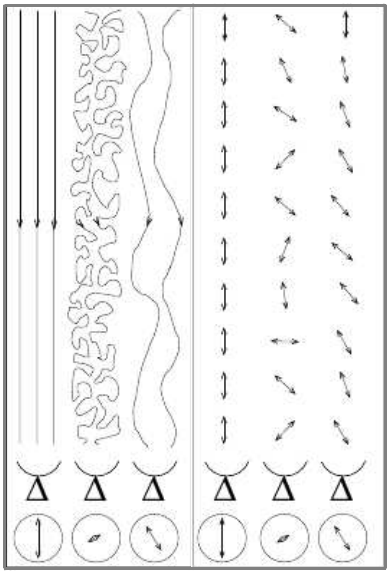

Figure 1.5: Polarization from the different magnetic field types, reproduced from Haverkorn, M. (2002). The three different lines of sight in the left hand panel describe situations with a regular field, an isotropic random field, and a combination of a regular and isotropic random field, respectively. The double-arrowed lines in the right hand panel represent the polarization vector at points along these lines of sight. The two groups of schematics at the bottom of each of the two panels represent the radio telescope and the resulting strength and direction of the measured polarization along the whole line of sight.

1.5 Current status of magnetic field knowledge in spiral galaxies

Our vantage point from within the Milky Way disk, near the Galactic mid-plane[4], allows for the study of magnetic fields in discrete objects on parsec (pc) and sub-parsec scales as well as large-scale field reversals along the Galactic radius. In the Galactic disk, the outer scale of fluctuations has a scale of $\lesssim$ 10 pc in the spiral arms and $\lesssim$ 100 pc in the interarm regions as measured from observations of *RM* by Haverkorn et al. (2008). However, the nature of the Galactic Center magnetic field (Ferrière 2009), the global azimuthal structure of the Galactic field (Men et al. 2008), and the number and locations of large-scale field reversals is still under debate (Haverkorn 2015). Observations of external (face-on) spiral galaxies provide 'zoomed-out' portraits of possible configurations for the Galactic magnetic field.

Magnetic fields in galaxies typically have micro-Gauss (μG) field strengths. The to-

[4]We are situated in the Orion-Cygnus arm and are currently at a height of 6 – 28 pc above the galactic plane (Joshi 2007).

tal magnetic field tends to be strongest in the inner few hundred parsecs of the galactic center region with an estimated range of field strengths from several tens of μG to as high as several milli-Gauss (mG). With the exception of starburst galaxies, whose nuclear starburst regions have some of the strongest total fields on account of intense star formation rates (SFRs) and SN rates (Beck 2009), high field strengths at the galactic center are thought to arise from a regular vertical field pervading the intercloud medium[5] (Ferrière 2011) as a result of dynamo action and/or from extreme turbulent activity in the galactic nucleus (Boldyrev & Yusef-Zadeh 2006). The concentration of molecular gas in a thin sheet parallel to the galactic plane, known as the central molecular zone (CMZ), may also compress regular magnetic fields to yield such high values, as is the case in the Milky Way. Assuming equipartition between magnetic field and cosmic ray energy densities, Niklas & Beck (1997) inferred an average total magnetic field strength of $9 \pm 3\,\mu$G for a sample of 74 spiral galaxies. Total magnetic field strengths of $10 - 15\,\mu$G are typical of 'grand-design' spiral galaxies with high SFRs such as M51 (Fletcher et al. 2011) and NGC 6946 (Beck 2007). The strength of the ordered magnetic fields in spiral galaxies are typically $1 - 5\,\mu$G but can be higher in grand-design spiral galaxies perhaps as a result of a more efficient galactic dynamo. In the spiral arms, the regular field is weaker and the turbulent field is stronger, probably due to star-forming processes and expansion of SNRs tangling the field (Beck 2001). Moreover, the strength of the ordered field (regular field plus anisotropic turbulent field) is at least five times weaker than the observed field strength of the isotropic turbulent field in the spiral arms (Beck & Wielebinski 2013). In between the spiral arms the regular field may be much stronger than the turbulent field and sometimes forms so called 'magnetic arms' as in NGC 6946 (Beck et al. 1996). In these interarm regions, the strength of the ordered field is about half to twice the strength of the disordered field (Beck & Wielebinski 2013). In general, the strength of the ordered field in the halo is comparable to the strength of the regular field in the disk (Krause 2014).

1.5.1 Spiral galaxies seen face-on

Observations of face-on spiral galaxies show a large-scale spiral field along the disk plane that is aligned with the spiral arms. The two most common magnetic field configurations observed are in fact the two lowest modes most easily excited by a galactic dynamo. These are the axisymmetric mode and the bisymmetric mode shown in Fig. 1.6. Higher modes may also be present but would have small amplitudes. Possible modes of magnetic fields in the halo are the symmetric, 'quadrupolar', or even-parity field and the anti-symmetric, 'dipolar', or odd-parity field as shown in Fig. 1.7. In the following, we refer to the vertical and horizontal magnetic field components as poloidal and toroidal, respectively. The symmetric field in the left-hand panel of Fig. 1.7 has a reversal in the direction of the poloidal component across the galactic plane and a toroidal component whose direction is the same above and below the plane. The anti-symmetric field in the right-hand panel of Fig. 1.7 has a poloidal component that runs through the galactic plane and a toroidal component that reverses directions above and below the plane. The actual mechanisms governing the

[5] Composed of the WNM, WIM, and HIM.

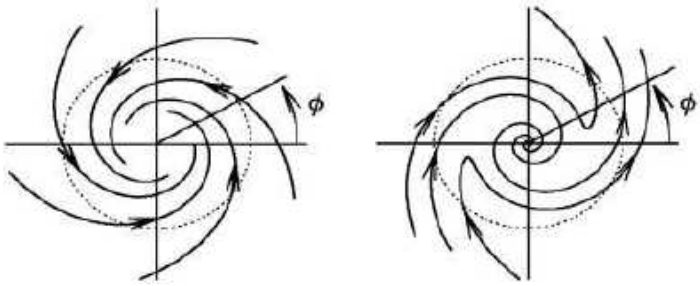

Figure 1.6: Illustration of axisymmetric and bisymmetric regular magnetic field configurations in the disk, respectively, reproduced from Widrow (2002).

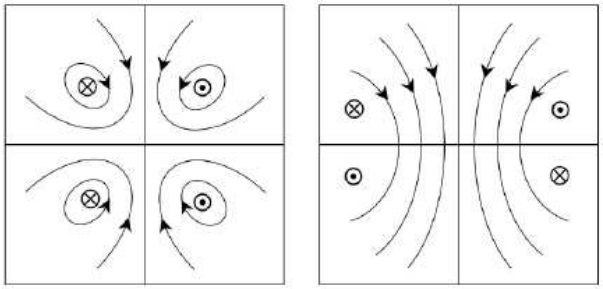

Figure 1.7: Illustration of symmetric and anti-symmetric regular magnetic field configurations in the halo reproduced from Haverkorn (2014).

structure of magnetic fields in galaxy halos still remains to be better understood.

Beck & Wielebinski (2013) provide a comprehensive compilation of magnetic field structure in both the disk and halo of spiral galaxies in their "catalog of radio polarization observations of nearby galaxies".

1.5.2 Spiral galaxies seen edge-on

In the Krause (2014) sample of 11 nearby edge-on galaxies of different Hubble type and covering a wide range in SFR, a disk-parallel field near the disk plane is observed which fans out from the disk at large vertical distances. Vertical field components that form an 'X-shape' pattern are observed in the halo. An outflow from the disk, such as a galactic wind, that transports the magnetic field from the disk to the halo may cause this morphology. A galactic dynamo may also be involved.

1.6 This thesis

In this thesis we reconstruct properties of magnetic fields in the disks and halos of spiral galaxies by means of the polarization of synchrotron radiation. Specifically, we use the polarization fraction as a diagnostic. The goal of this research project has been to infer the structure of the magnetic field across various angular scales in our own Galaxy (Chapter 2) and the strength and structure of the magnetic field in the disk and halo of external galaxies (Chapters 3 - 5) from the WIM phase of the ISM.

The main scientific objectives along with the areas to which this thesis has contributed to can be summarized as follows:

Chapter 2

Investigation of the spatial scales of polarization structures in terms of the energy distribution of the magnetic field in the Milky Way using statistical methods. The power spectra of diffuse synchrotron polarized intensity have been studied by a number of radio polarization surveys at various Galactic longitudes and latitudes, observing wavelengths, and angular scales (Haverkorn et al. 2003; Stutz et al. 2014). However, the interpretation of the values of these power spectra is complicated by the dependence of the radio observables on the magnetic field, outer scale of turbulence, thermal electron density distribution, cosmic ray electron density distribution, and path length.

Chapters 3 & 4

Development of methodology for describing the cumulative effects of various depolarization mechanisms and subsequent application of methodology to constrain magnetic field strengths in the spiral galaxy M51. Previous depolarization models have treated depolarization as arising solely from Faraday rotation. Furthermore, it has been customary to define RM by a simple linear relationship between polarization angle change with the square of the observing wavelength as $RM = d\Psi/d\lambda^2$ based on Eq. (1.2). However, if synchrotron emission and the Faraday-rotating medium are mixed or alternating along the line of sight, this simple linearity no longer holds. This probably applies to the majority of Faraday rotation measurements of the diffuse synchrotron emission in galaxies.

Chapter 5

Examination of a physically motivated 'X-shape' regular magnetic field model for constraining magnetic field strength and structure in the spiral galaxy NGC 6946. Traditionally, dipole and quadrupole magnetic fields have been used to model the magnetic field in the halo. The dipole and quadrupole magnetic fields are the second and third terms, respectively, representing the total magnetic field in a multipole expansion[6] in powers of inverse radial distance for a spherically symmetric

[6]The first term of the multipole expansion is zero as there are no magnetic monopoles.

object. This expansion assumes that the magnetic field can be represented as the gradient of a scalar magnetic potential resulting from having zero current. With zero current, there is no force to act on the magnetic field. Although the halo is an almost spherical rotating body, the galaxy encloses an interstellar plasma which enables cross-field electric currents to flow, making the magnetic field generally not force-free, and, thereby, causing departures from the pure dipole and quadrupole geometries. This necessitates consideration of more complex geometries.

In Chapter 2, statistically independent realizations of physical 3D random magnetic fields with prescribed power spectra are generated. The properties of this random field are assumed to reproduce some of the observed properties of turbulence in the ISM. The turbulence is assumed to be purely isotropic and representative of a high galactic latitude environment. These magnetic field 'cubes' are then used to simulate radio observables of Stokes I, Q, U, and polarized intensity P at several physically motivated observing wavelengths together with varying parameters of cosmic ray electron density, outer scale of fluctuations, and integrated path length. Subsequently, the angular power spectrum (APS) prescription of Haverkorn et al. (2003) is used to measure the statistical angular (auto)correlations for each of these resulting radio observables. The spectral indexes of the observables are α_I, α_Q, α_U, α_P, respectively. Two aspects in particular contribute to the novelty of our approach: (1) we use the recent method of Stepanov et al. (2014) to search for imprints of point-wise equipartition and pressure equilibrium between cosmic ray electrons and local magnetic field energy density on the power spectra of radio observables and (2) we simulate a realistic cone-like field of view with diverging sight lines as expected from radio sources that are at most only at a few kpc distance. We find that α_I traces the underlying magnetic field power spectrum but that it may not be possible to use α_I to identify the actual magnetic field power spectrum due to measurement uncertainties. We also find that α_Q, α_U, and α_P can not be used to determine the magnetic field power spectrum since a wide range of values arise from a single underlying magnetic field power spectrum on account of a degenerate dependence on the parameters described above. Furthermore, assumptions of equipartition/pressure equilibrium do not affect the polarization spectral indices but do have an effect on the amplitude of the power spectrum. An interesting further prediction of our model is that the power spectra of Q, U, and P may have a frequency dependent break whose angular scale depends on parameters of the turbulence and hence can be a useful diagnostic in establishing turbulence parameters. This is necessary to consider as a frequency dependent break has been traditionally interpreted in the literature as evidence for a non-singular turbulent power spectrum whereas in our models it arises from a single turbulent power spectrum. Moreover, flat or inverted power spectra at low frequencies ($\leq$ 200 MHz) are obtained which could be detected with LOFAR and MWA.

In Chapter 3, we develop an analytical framework for treating depolarization arising from the superposition of all three distinct magnetic field types occurring along the line of sight. We account for the combined action of wavelength-dependent and wavelength-independent synchrotron depolarization mechanisms in a face-on galaxy, modeled as a synchrotron-emitting and Faraday-rotating multilayer magneto-ionic medium.

In particular, we are able to probe the different depolarization effects of the two distinct types of turbulent magnetic field which was previously a black-box with previous approaches in the literature. Subsequently, as a proof-of-concept, a small-region case study is performed in the grand-design, face-on spiral galaxy M51. This allows for a direct statistical comparison with the observed polarization maps at the observing wavelengths. Seventeen distinct model types are constructed, comprised of all possible combinations of a regular, isotropic turbulent, and anisotropic turbulent magnetic fields in each of the disk and halo. Although we only had three observing wavelengths to work with, our approach was able to reduce the original pool of the 17 distinct model types to a smaller subset of models that all required the presence of turbulent magnetic fields in both the disk and the halo. Such models are a natural next step in complexity (Heald et al. 2014), indicative of the type of investigations that can be performed with large samples of galaxies observed with wideband, multichannel polarization capability such as with the upcoming SKA.

In Chapter 4, we apply the developed methodology to the entire M51 galaxy. We assess the robustness of our approach via a bootstrap technique. Assuming independence of magnetic field strengths on azimuth provides sufficient constraints to gauge the regular and turbulent magnetic strengths. We find that a model with all three field types in the disk and a regular plus isotropic turbulent field in the halo fits best to the data. Furthermore, the total magnetic field strength and the regular and turbulent magnetic field strengths in the disk are all several times higher than in the halo. Values of magnetic fields are in agreement with those previously inferred in the literature which gives confidence to our methodology. Moreover, our multilayer approach confirms the result from previous literature that the far-side of the halo is completely depolarized and does not contribute to depolarization.

In Chapter 5, we construct a so called 'X-shape' magnetic field, as a model for the regular field in the almost face-on spiral galaxy NGC 6946. This field is divergence-free by construction and, thus, physical. An X-shape magnetic field gives rise to an X-shape polarization pattern, typically observed in edge-on spiral galaxies, and is thought to be common in spiral galaxies. The global 3D magnetic field morphology of the best-fit model is explicitly shown along with this model's predicted average magnetic field strength which is consistent with earlier estimates in the literature. Our model requires additional complexity to fit the data well.

Bibliography

Armstrong, J. W., Rickett, B. J., & Spangler, S. R. 1995, ApJ, 443, 209

Beck, R. 2001, Space Sci. Rev., 99, 243

Beck, R. 2004, Ap&SS, 289, 293

Beck, R. 2007, A&A, 470, 539

Beck, R. 2009, Astrophysics and Space Sciences Transactions, 5, 43

Beck, R., Brandenburg, A., Moss, D., Shukurov, A., & Sokoloff, D. 1996, ARA&A, 34, 155

Beck, R. & Wielebinski, R. 2013, Magnetic Fields in Galaxies, ed. T. D. Oswalt & G. Gilmore, 641

Boldyrev, S. & Yusef-Zadeh, F. 2006, ApJ, 637, L101

Breitschwerdt, D., McKenzie, J. F., & Voelk, H. J. 1991, A&A, 245, 79

Breitschwerdt, D., McKenzie, J. F., & Voelk, H. J. 1993, A&A, 269, 54

Ferrière, K. 2009, A&A, 505, 1183

Ferrière, K. 2011, in IAU Symposium, Vol. 271, IAU Symposium, ed. N. H. Brummell, A. S. Brun, M. S. Miesch, & Y. Ponty, 170–178

Ferrière, K. M. 2001, Reviews of Modern Physics, 73, 1031

Fletcher, A., Beck, R., Shukurov, A., Berkhuijsen, E. M., & Horellou, C. 2011, MNRAS, 412, 2396

Hanasz, M., Kowal, G., Otmianowska-Mazur, K., & Lesch, H. 2004, ApJ, 605, L33

Haverkorn, M. 2014, ArXiv e-prints

Haverkorn, M. 2015, in Astrophysics and Space Science Library, Vol. 407, Astrophysics and Space Science Library, ed. A. Lazarian, E. M. de Gouveia Dal Pino, & C. Melioli, 483

Haverkorn, M., Brown, J. C., Gaensler, B. M., & McClure-Griffiths, N. M. 2008, ApJ, 680, 362

Haverkorn, M. & Heesen, V. 2012, Space Sci. Rev., 166, 133

Haverkorn, M., Katgert, P., & de Bruyn, A. G. 2003, A&A, 403, 1045

Haverkorn, M. 2002, PhD thesis, Leiden University, The Netherlands

Heald, G., Beck, R., de Blok, W. J. G., et al. 2014, in Proceedings of Advancing Astrophysics with the Square Kilometre Array (AASKA14). 9 -13 June, 2014. Giardini Naxos, Italy., 106

Hennebelle, P. & Falgarone, E. 2012, A&A Rev, 20, 55
Iacobelli, M., Haverkorn, M., & Katgert, P. 2013, A&A, 549, A56
Joshi, Y. C. 2007, MNRAS, 378, 768
Krause, M. 2014, ArXiv e-prints
Kulpa-Dybeł, K., Nowak, N., Otmianowska-Mazur, K., et al. 2015, A&A, 575, A93
Landecker, T. L. 2012, Space Sci. Rev., 166, 263
Le Roux, E. 1961, Annales d'Astrophysique, 24, 71
Mao, S. A., Zweibel, E., Fletcher, A., Ott, J., & Tabatabaei, F. 2015, ApJ, 800, 92
Men, H., Ferrière, K., & Han, J. L. 2008, A&A, 486, 819
Mulcahy, D. D., Horneffer, A., Beck, R., et al. 2014, A&A, 568, A74
Niklas, S. & Beck, R. 1997, A&A, 320, 54
Parker, E. N. 1955, ApJ, 122, 293
Parker, E. N. 1966, ApJ, 145, 811
Parker, E. N. 1992, ApJ, 401, 137
Schekochihin, A. A. & Cowley, S. C. 2007, Turbulence and Magnetic Fields in Astrophysical Plasmas, ed. S. Molokov, R. Moreau, & H. K. Moffatt (Springer), 85
Stepanov, R., Shukurov, A., Fletcher, A., et al. 2014, MNRAS, 437, 2201
Stutz, R. A., Rosolowsky, E. W., Kothes, R., & Landecker, T. L. 2014, ApJ, 787, 34
Tielens, A. G. G. M. 2005, The Physics and Chemistry of the Interstellar Medium
Widrow, L. M. 2002, Reviews of Modern Physics, 74, 775
Wolleben, M., Fletcher, A., Landecker, T. L., et al. 2010, ApJ, 724, L48